

## Multi-criteria shape design of crane-hook taking account of estimated load condition

Takao Muromaki<sup>\*1</sup>, Kazuyuki Hanahara<sup>2a</sup> and Yukio Tada<sup>2b</sup>

<sup>1</sup>*Mechanical Engineering, Maizuru National College of Technology,  
234 Siroya, Maizuru, Kyoto, 625-8511, Japan*

<sup>2</sup>*Graduate School of System Informatics, Kobe University, 1-1 Rokkodai, Nada, Kobe, 657-8501, Japan*

*(Received May 1, 2012, Revised May 10, 2014, Accepted May 18, 2014)*

**Abstract.** In order to improve the crane-hook's performance and service life, we formulate a multi-criteria shape design problem considering practical conditions. The structural weight, the displacement at specified points and the induced matrix norm of stiffness matrix are adopted as the evaluation items to be minimized. The heights and widths of cross-section are chosen as the design variables. The design variables are expressed in terms of shape functions based on the Gaussian function. For this multi-objective optimization problem with three items, we utilize a multi-objective evolutionary algorithm, that is, the multi-objective Particle Swarm Optimization (MOPSO). As a common feature of obtained solutions, the side views are tapered shapes similar to those of actual crane-hook designs. The evaluation item values of the obtained designs demonstrate importance of the present optimization as well as the feasibility of the proposed optimal design approach.

**Keywords:** optimal design; crane-hook; finite element method; Gaussian; MOPSO

---

### 1. Introduction

An excavator is one of the fundamental machines used for construction work. Recently, excavators having a crane-hook are widely used in construction work sites. One reason is that there are work sites where the crane trucks for suspension work are not available because of the narrowness of the working site; an excavator has superior serviceability to a crane truck in general. Another reason is that such an excavator is convenient because they can perform the conventional digging tasks as well as the hanging works mentioned above. Fig. 1(a) shows a sample image of excavator with crane-hook and (b) shows the close-up image of its bucket part where the crane-hook is attached.

Contrary to its convenience, there are cases that the crane-hooks are damaged during some kind of hanging works. Fig. 2(a) shows a typical crane-hook and (b) shows its failed sample to be repaired. This type of hook can be used to suspend objects whose weight is up to 2.9t. In Fig. 2(b),

---

\*Corresponding author, M. Eng., E-mail: [t.muromaki@maizuru-ct.ac.jp](mailto:t.muromaki@maizuru-ct.ac.jp)

<sup>a</sup>Ph.D., E-mail: [hanahara@cs.kobe-u.ac.jp](mailto:hanahara@cs.kobe-u.ac.jp)

<sup>b</sup>Professor, E-mail: [tada@cs.kobe-u.ac.jp](mailto:tada@cs.kobe-u.ac.jp)

we can see that the locking apparatus, called latch, is left open. From the view point of safety, such failure must be avoided. Improvement of the performance and the service life is important; the real conditions of such suspension tasks in practical environment are, however, still unclear. It is necessary to consider the design problem which involves physical and geometrical uncertainties in some degree.

In order to develop a high quality product that is supposed to be used under uncertain condition, there are two typical approaches. One is the robust optimal design considering various kinds of load conditions as well as other uncertain factors such as the model error. The other is the optimal design based on a criterion specialized to take account of the estimated failure factor. In the former approach, a variety of robust design methods are proposed in the literature (Marano *et al.* 2010, Vissarion and Nikos 2009, Zhiping *et al.* 2007, Chris and Sara 2001). The key point of this approach is the determination or formulation of the uncertainties. In the latter approach, identification of the cause of failure is one of the key issues for the purpose of safety improvement. Several failure detection methods are proposed in the past (Xiang *et al.* 2011, Lam and Ng 2009). However, almost all failed structures themselves have no information about the load conditions during their service life. We developed a failure estimation approach that uses the failure structure images. Our previous work (Muromaki *et al.* 2012) gives the estimation of load condition in the form of probability distribution. On the basis of the distribution, we formulate a criterion for optimal design that takes account of the load condition uncertainty. We deal with the following three evaluation items for the optimal design.

- structural weight
- strength against the specified load condition
- robustness for unspecified load condition

The first item is selected for achievement of the light weight. The second item is selected for evaluation of the strength against a critical load condition leading to the damage of the hook. The third item is selected for achievement of the high-stiffness against unspecified and multiple load conditions. The latter two items reflect the load condition obtained in the previous study. It is important to evaluate the mechanical rationality and the material cost simultaneously. We formulate the multi-criteria design problem with these three items. This problem is solved by using the multi-objective particle swarm optimization (MOPSO). We show the common characteristics in the obtained solutions and discuss the difference in shape between the obtained solutions and actual designs.

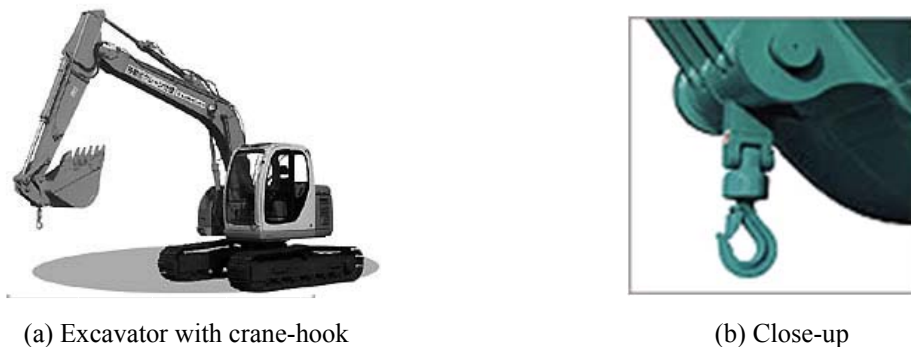


Fig. 1 Sample image of excavator and its close-up

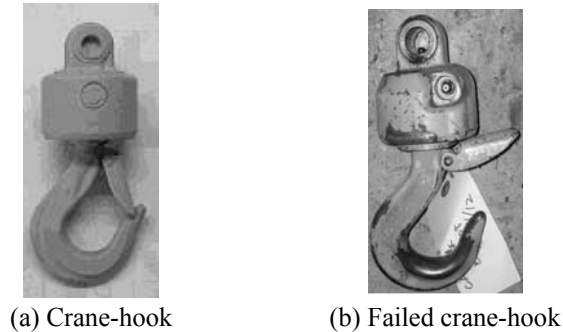


Fig. 2 Typical crane-hook and failed sample

## 2. Modeling of crane-hook

### 2.1 Finite element model of crane-hook

We construct a finite element model of crane-hook based on one of its actual designs. Fig. 3 shows the design drawing of crane-hook adopted as the reference. Its cross-sectional shapes are illustrated by the shaded area at two positions. One is the lowest center position “E” where the load is applied in conventional suspension work. The other is the position “D” where the largest stress occurs in the typical work. This area is usually called “critical section”. These cross-sectional shapes, called “T shape”, have been achieved by the expert engineers empirically.

The crane-hook model adopted in this study is shown in Fig. 4. This model is constructed based on Fig. 3. The dimensions of the crane-hook dealt with in this study are indicated in Table 1. As indicated in Fig. 4, the latch part is omitted in the adopted model because it does not contribute to supporting the applied load. The center line of the model indicated by the broken line is represented as follows:

- a straight line from the tip-end point “G” to point “F”
- a circular arc from point “F” to point “C”
- a piecewise linear line from point “C” to point “A”

In the interval between points “A” and “C”, the positions of the representative points are determined by referring to the actual design shown in Fig. 3.

Fig. 5 shows the layered model of the section used in this study. This model is constructed of  $N_d$  layers. The height of cross-section is specified by “ $h$ ”. The height of each layer is assigned evenly. The width of each layer is specified by “ $b_i$ ” ( $i=1, \dots, N_d$ ). By changing these widths  $b_i$ , we can represent various cross-sectional shapes.

A finite element model is developed based on the one dimensional beam element. The crane-hook model is divided into  $N_e$  elements. Fig. 6(a) shows the finite element model and (b) is a slice of the model. The shaded area represents the side of the element. In the elastic deformation analysis, the equilibrium equation is obtained by means of the conventional finite element analysis approach and expressed as

$$\mathbf{F} = \mathbf{K}\mathbf{U} \quad (1)$$

where  $\mathbf{F}$ ,  $\mathbf{K}$  and  $\mathbf{U}$  are the external force vector, the stiffness matrix and the displacement vector. Given a specified external force vector and boundary conditions, the corresponding deformation of the crane-hook is calculated on the basis of Eq. (1).

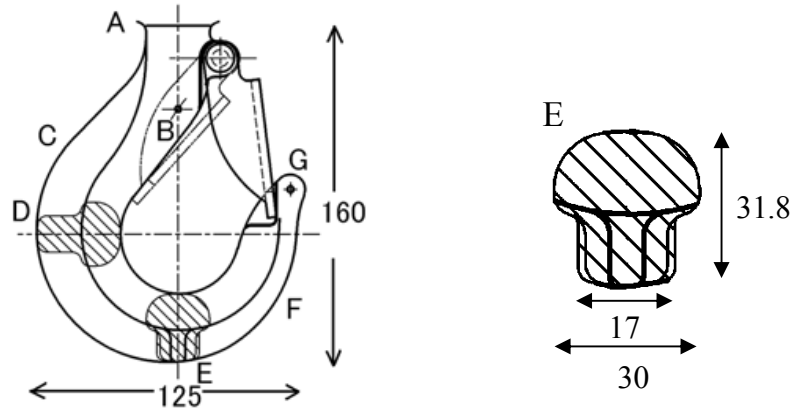


Fig. 3 Design drawing of crane-hook

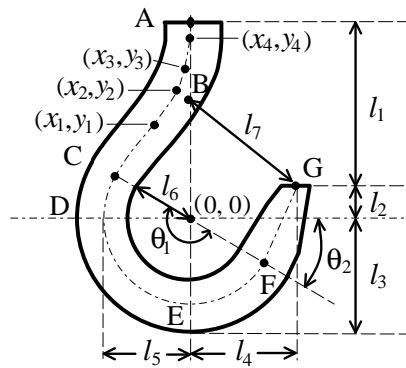


Fig. 4 Crane-hook model

Table 1 Dimension of crane-hook model

parameter	value	parameter	value
$l_1$	80 [mm]	$l_2$	20 [mm]
$l_3$	60 [mm]	$l_4$	54 [mm]
$l_5$	44 [mm]	$l_6$	28 [mm]
$l_7$	66 [mm]		
$\theta_1$	180°	$\theta_2$	30°
$(x_1, y_1)$	(-22, 50)	$(x_2, y_2)$	(-8, 70)
$(x_3, y_3)$	(-4, 80)	$(x_4, y_4)$	(0, 9)

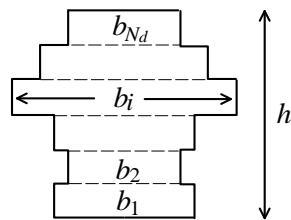


Fig. 5 Layered model of cross section

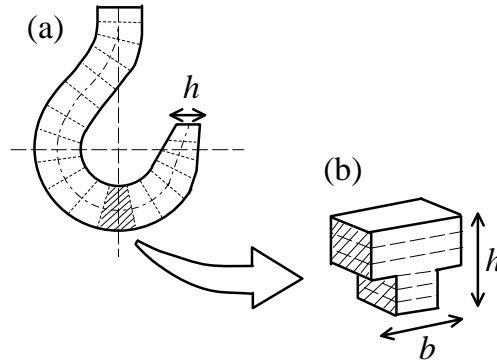


Fig. 6 FE model based on 1-D beam element

## 2.2 Elasto-plastic deformation analysis

In Fig. 2(b), we can see the permanent deformation of the failed hook. In order to improve the safety and strength of the crane-hook, it is important to do the elasto-plastic deformation analysis. We discuss a crane-hook design based on the elasto-plastic deformation analysis. In our analysis, the stress-strain relationship of the material is approximated by a piecewise linear function as shown in Fig. 7 (Crisfield 1991). In this figure,  $E_1$  is the Young's modulus,  $E_2$  is the tangent modulus and  $\bar{\sigma}$  is the yield stress. The dashed line indicates the relationship in the unloading process; the tangent modulus in this case is assumed to be equal to the Young's modulus  $E_1$ . In order to calculate the displacement of finite element model, we utilize the incremental solution scheme (Crisfield 1991). The incremental formulation is expressed as

$$\Delta F = K_t \Delta U \quad (2)$$

where  $\Delta F$ ,  $K_t$  and  $\Delta U$  are the incremental force vector, the tangent stiffness matrix and the incremental displacement vector, respectively. The tangent stiffness matrix  $K_t$  takes over the role of the stiffness matrix in elastic analysis. It relates small change in force to small change in displacement. The matrix  $K_t$  takes the form

$$K_t = K_t(U), K_t(\mathbf{0}) = K \quad (3)$$

where  $K$  is the elastic stiffness matrix used in the linear elastic analysis as Eq. (1). The total displacement is computed by the sum of the incremental displacements  $\Delta U$ .

$$U = \sum \Delta U \quad (4)$$

In the assessment process of the yielding, we utilize the layered approach (Owen and Hinton 1980). In this approach the beam element is subdivided into layers, as shown in Fig. 5. A layer element is determined to be in yield state as a whole in the case that the central stress of the layer reaches the material yield stress. The stiffness values of the elements are determined according to the stress-strain relationship shown in Fig. 7.

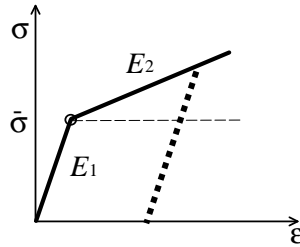


Fig. 7 Adopted stress-strain relationship model

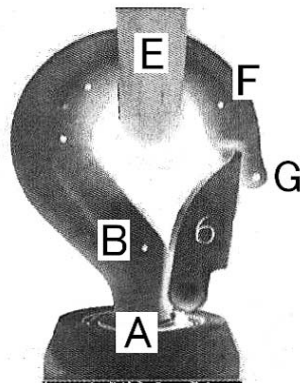


Fig. 8 Stretch experiment of hook

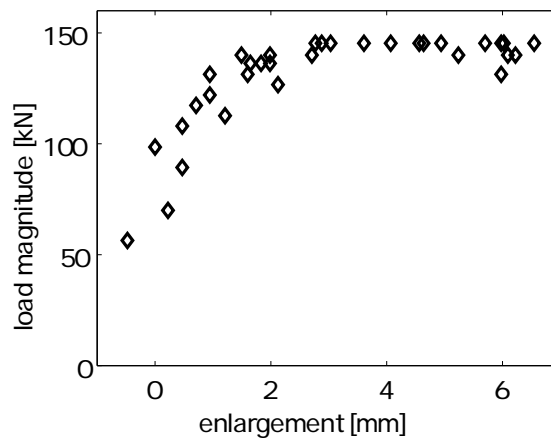


Fig. 9 Relation between applied load and enlargement of displacement

### 2.3 Estimation of physical parameters

As shown in Fig.7, the stress-strain relationship has three parameters: the Young's modulus  $E_1$ , the tangent modulus  $E_2$  and the yield stress  $\bar{\sigma}$ , which must be determined. We estimate them based on experimental data. The stretch experiment of crane-hooks conducted is as follows. A load is applied at the point "E" of crane-hook shown in Fig. 8. We measure the distance between points

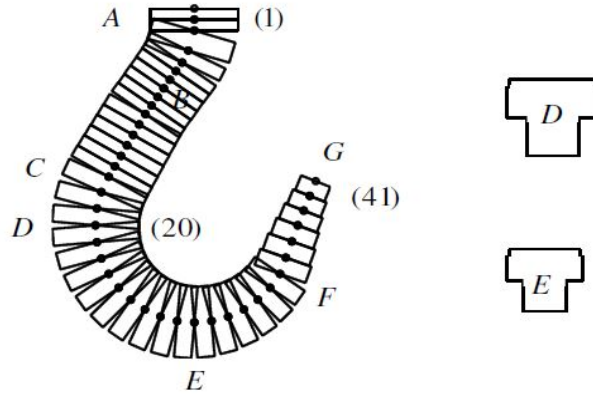


Fig. 10 FEM model and its sections for parameter estimation: the reference design

“B” and “G” at various load conditions and obtain the enlargement of the distance. Fig. 9 shows the experimental result. The ordinate and the abscissa represent the magnitude of load [kN] and the enlargement of distance between point “B” and “G” [mm], respectively. On the basis of the obtained data, the plastic deformation is determined to occur at a load around 120 [kN]. The nominal load of the crane-hook dealt with in this study is 29 [kN], thus we can see that the nominal load is far below the plastic deformation area.

In order to determine the material parameters based on the experimental data, we formulate a minimum square error problem. The data points in Fig. 9 are represented as  $(f_i, y_i)$ , where  $f_i$  is the  $i$ -th magnitude of load and  $y_i$  is the enlargement between “B” and “G” for the load  $f_i$ . The enlargement corresponding to the load  $f_i$  can also be obtained by means of the calculation based on the parameter set  $\{E_1, E_2, \bar{\sigma}\}$  and the FEM model shown in Fig. 10; the FEM model has the dimension and the cross-sectional shape corresponding to the actual design of hook shown in Fig. 3. We represent the calculated enlargement as  $\hat{y}_i$ . The relation can be expressed as follows

$$\hat{y}_i = \hat{y}_i\{f_i, E_1, E_2, \bar{\sigma}\} \quad (5)$$

The minimum square error problem for the parameter estimation is set as follows

$$\text{Minimize } \sum_i (y_i - \hat{y}_i)^2 \quad \text{with respect to } E_1, E_2, \bar{\sigma} \quad (6)$$

Table 2 shows the candidates of these parameters and the results of the error-minimization. The results are obtained by the exhaustive search and are shown in the lowest row. In the following, we utilize these estimated values for the FEM analysis.

### 3. Shape optimization

#### 3.1 Setting of criteria and formulation of optimization problem

We explain the formulation of criteria that evaluate the crane-hook design. In order to improve

Table 2 Range of parameters and results of error-minimization

	$E_1$ [GPa]	$E_2$ [GPa]	$\bar{\sigma}$ [MPa]
range	190~270	1~50	100~600
candidates	190	1	100
	200	3	150
	210	5	200
	⋮	8	⋮
	260	10	550
	270	15	600
		20	
		⋮	
		45	
		50	
estimated	260	8	350

the performance of crane-hook, we employ the following criteria:

- (i) structural weight
- (ii) displacement of specified points under specified load condition
- (iii) ratio between displacement norm and possible load norm

Criterion (i) is selected for the achievement of the light weight. Light weight is important for the saving of material cost and the compactness. The structural weight  $J_1$  is formulated as

$$J_1 = \sum_{i=1}^{N_e} \rho A_i l_i \quad (7)$$

where  $N_e$  is the number of FE elements,  $\rho$  is the material density,  $A_i$  is the cross-sectional area of  $i$ -th element and  $l_i$  is the element length.

Criterion (ii) is selected for the evaluation of the strength against the elasto-plastic deformation. This criterion is calculated in terms of the displacement of specified points under a given load condition. The adopted load condition for this criterion is shown in Fig. 11 as  $\mathbf{P}$ . The load applied position is not at the lowest point of the crane-hook but at the right-hand shifted point from the lower center. The load direction is not normal to the contour curve but leftward. This load condition is set based on our previous work (Muromaki *et al.* 2012). The failure estimation results of the report are shown in Fig.12. This figure illustrates the probability of load applied position by gray-scale level. Their gray-scale levels are assigned by the estimated density function, dark part for high probability and light part for low probability. The position and direction of load vector  $\mathbf{P}$  is determined by means of the estimated density functions. Under the applied load vector  $\mathbf{P}$ , we calculate the displacement at two parts. One is the displacement at the lower center point “E” and the other is the enlargement of the displacement between the points “B” and “G”. Fig. 13(a) shows the parts where displacements are evaluated. Criterion (ii) is formulated as

$$J_2 = \|\mathbf{U}_E\| + \left| \hat{BG} - \overline{BG} \right| \quad (8)$$

where  $\mathbf{U}_E$  is the nodal displacement vector at the point “E” obtained by the elasto-plastic

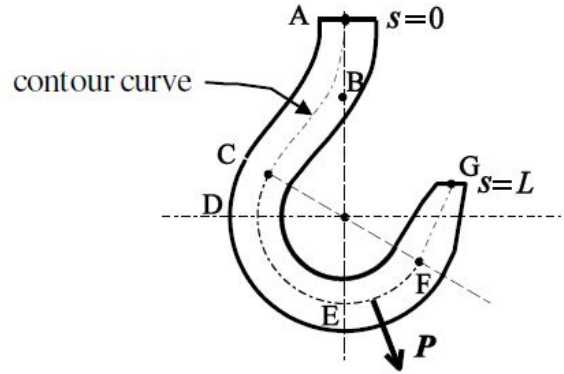


Fig. 11 Load condition for criterion (ii) and local curvilinear coordinate  $s$

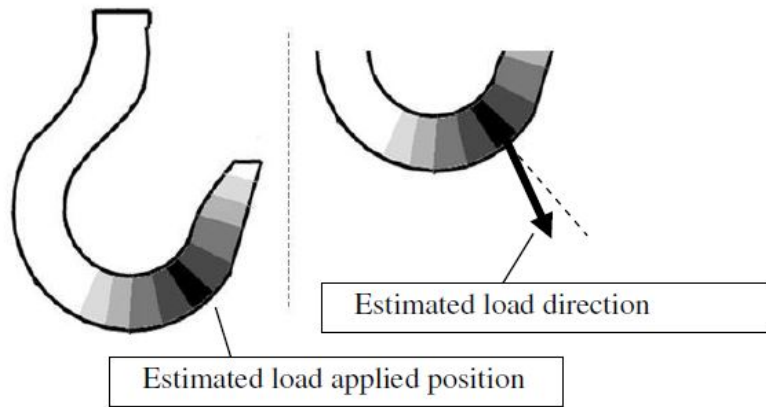


Fig.12 Critical load applied position and load direction

deformation analysis explained in section 2.2,  $\widehat{BG}$  is the distance between the points “B” and “G” under the loading condition and  $\overline{BG}$  is the initial distance without load. The initial distance is represented by the symbol  $l_7$  in Fig. 4 and its value is shown in Table 1.

Criterion (iii) is selected for evaluation of the robustness of structure against unspecified multiple load conditions. We aim to minimize the deformation to unspecified loads averagely. For this evaluation, we adopt the ratio between the norm of the global displacement vector and the norm of the possible load vector. The robustness of the structure is evaluated in terms of the maximum value of the ratio. The possible load vector is represented by  $\tilde{F}$ . This vector is corresponding to an arbitral force acting on some specific points. The maximum ratio  $J_3$  is expressed as

$$J_3 = \max_{F \neq 0} \frac{\|U\|}{\|\tilde{F}\|} \tag{9}$$

$$U = K^{-1}F, \quad F = B_v \tilde{F} \tag{10}$$

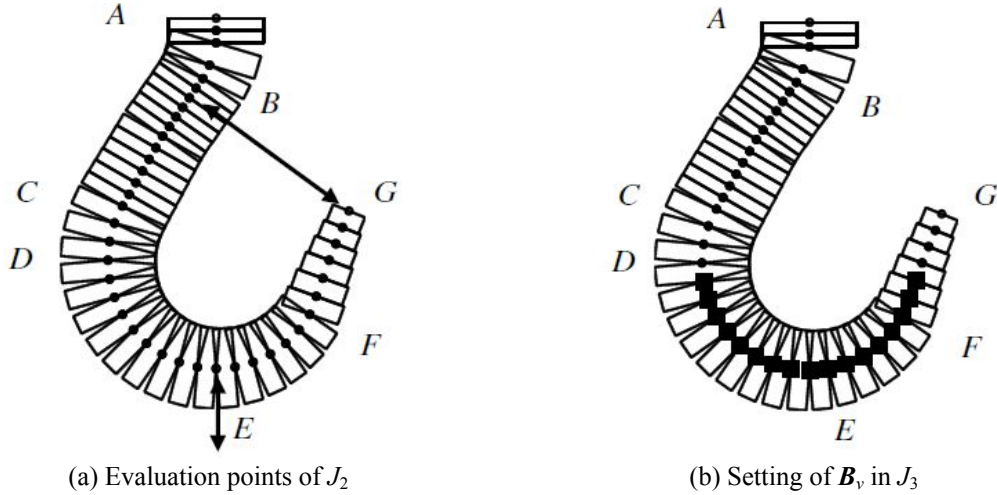


Fig. 13 Specification of criteria (ii) and (iii)

where  $\|\cdot\|$  represents the vector norm and  $\mathbf{K}$  is the elastic stiffness matrix in Eq.(1). The global force vector  $\mathbf{F}$  is associated with the possible load vector  $\tilde{\mathbf{F}}$  on the specific points by the Boolean matrix  $\mathbf{B}_v$ . The matrix  $\mathbf{B}_v$  specifies where the loads are applied, that is, the points shown in Fig.13(b) by the square marks. The maximum ratio is rewritten in the following form

$$J_3 = \max_{\tilde{\mathbf{F}} \neq 0} \frac{\|\mathbf{U}\|}{\|\tilde{\mathbf{F}}\|} = \max_{\tilde{\mathbf{F}} \neq 0} \frac{\|\mathbf{K}^{-1}\mathbf{F}\|}{\|\tilde{\mathbf{F}}\|} = \max_{\tilde{\mathbf{F}} \neq 0} \frac{\|\mathbf{K}^{-1}\mathbf{B}_v\tilde{\mathbf{F}}\|}{\|\tilde{\mathbf{F}}\|} \quad (11)$$

The magnitude of  $\|\tilde{\mathbf{F}}\|$  is normalized to unity. In the current study, instead of searching the maximum value directly, we utilize the matrix norm. According to the maximum principle of the eigenvalue, the maximum value of this function is calculated as the matrix norm induced by the Euclidean vector norm  $\|\cdot\|_2$  (Roger and Charles 1985). Criterion (iii) is then calculated as

$$J_3 = \|\mathbf{K}^{-1}\mathbf{B}_v\|_2 = \max\{\sqrt{\lambda} : \lambda \text{ is an eigenvalue of } (\mathbf{K}^{-1}\mathbf{B}_v)^T(\mathbf{K}^{-1}\mathbf{B}_v)\} \quad (12)$$

where superscript  $T$  denotes the transpose operation. This criterion represents a displacement-force ratio and the unit is [m/N].

In this study, the design variables of crane-hook are the parameters of cross-section of FEM elements. As shown in Fig. 5 and Fig. 6, the parameters of cross-section are the height and layer widths. These design variables are represented as the functions of the local coordinate  $s$  attached at the contour curve of hook, as  $h(s)$ ,  $b_i(s)$  ( $0 \leq s \leq L$ ), where  $L$  is the length of the contour curve. The coordinate  $s$  is indicated in Fig. 11. The start point of  $s$  is the base point "A" and the end point is the tip point "G". The height of the layers at  $s$  is evenly assigned as  $h(s)/N_d$ .

The multi-objective optimal design problem of the crane-hook is then expressed as follows

$$\begin{aligned} &\text{Minimize } \frac{J_1}{J_1}, \frac{J_2}{J_2}, \frac{J_3}{J_3} && \text{with respect to } h(s), b_i(s) \\ &\text{subject to } h_L \leq h(s) \leq h_U, b_L \leq b_i(s) \leq b_U, J_2 \leq U_{\max} \end{aligned} \quad (13)$$

where  $\underline{J}_1$ ,  $\underline{J}_2$  and  $\underline{J}_3$  are the evaluation item values for normalization. We adopt the FEM model of crane-hook shown in Fig. 10, called “reference design”, for this normalization. The values  $\underline{J}_1$ ,  $\underline{J}_2$  and  $\underline{J}_3$  are calculated for the reference design. The constants  $h_L$  and  $b_L$  and  $h_U$  and  $b_U$  are the lower and upper bounds of the height and width, respectively. The constraint  $U_{\max}$  is the imposed allowable limit of the displacement. This constraint is adopted for excluding low-strength designs.

### 3.2 Design variables and their parametric representation

In this study, the design variables are the shape functions of height  $h(s)$  and widths  $b_i(s)$  of the cross-section. There are several kinds of methods that represent such shape functions as linear combination of basis functions (Vanderplaats 1979). We utilize the Gaussian function (Boyd and Wang 2009) to represent the design variables  $h$  and  $b_i$ . The shape functions are then expressed as

$$h(s) = \sum_{j=1}^{N_h} \alpha_j^h \exp\left(-\frac{(s - \mu_j^h)^2}{2(\beta_j^h)^2}\right) \tag{14}$$

$$b_i(s) = \sum_{j=1}^{N_b} \alpha_j^{b_i} \exp\left(-\frac{(s - \mu_j^{b_i})^2}{2(\beta_j^{b_i})^2}\right) \tag{15}$$

where  $\alpha$  is the scaling factor,  $\mu$  and  $\beta$  are the location of the peak and the standard deviation. The constants  $N_h$  and  $N_b$  are the number of Gaussian functions representing  $h$  and  $b_i$ , respectively. Fig. 14 shows example Gaussian functions and their superposition. The thinner lines represent individual Gaussian functions and the thicker line is the integrated function obtained by adding the two Gaussian functions. By introducing this representation, the shape functions  $h(s)$  and  $b_i(s)$  are represented in terms of the coefficients  $\alpha_j^h, \beta_j^h, \mu_j^h$  ( $j=1, \dots, N_h$ ) and  $\alpha_j^{b_i}, \beta_j^{b_i}, \mu_j^{b_i}$  ( $j=1, \dots, N_b$ ). The optimization problem (13) is rewritten in the following form

$$\begin{aligned} \text{Minimize } \tilde{J}_1, \tilde{J}_2, \tilde{J}_3 \quad & \text{with respect to } \alpha_j^h, \beta_j^h, \mu_j^h, \alpha_j^{b_i}, \beta_j^{b_i}, \mu_j^{b_i} \\ & (i = 1, \dots, N_d, j = 1, \dots, N_h \text{ or } N_b) \\ \text{subject to } & h_L \leq h(s) \leq h_U, b_L \leq b_i(s) \leq b_U, J_2 \leq U_{\max} \end{aligned} \tag{16}$$

where  $\tilde{J}_1 \equiv J_1/\underline{J}_1$ ,  $\tilde{J}_2 \equiv J_2/\underline{J}_2$  and  $\tilde{J}_3 \equiv J_3/\underline{J}_3$ .

Researchers such as (Srirat *et al.* 2012) and (Iman *et al.* 2012) adopt only the coefficients  $\alpha$  in Gaussian basis functions as design variables, but we choose all the coefficients  $\alpha, \mu$  and  $\beta$  in Eqs. (14) and (15) as the design variables to be determined in our optimal design. The increase in the number of design variables is not convenient especially from the viewpoint of the computational cost in the optimization process; however, the adjustment of the coefficient  $\beta$  as well as  $\mu$  is crucial for the shape representation in terms of Eqs. (14) and (15) to express some shapes such as a near-flat shape A-C of the reference design shown in Fig. 10. In this case, the radial basis function representation is nonlinear in these design variables. However, the optimization method adopted in this study explained in the following, the particle swarm optimization, is a powerful algorithm suitably applicable to nonlinear optimization problems as well.

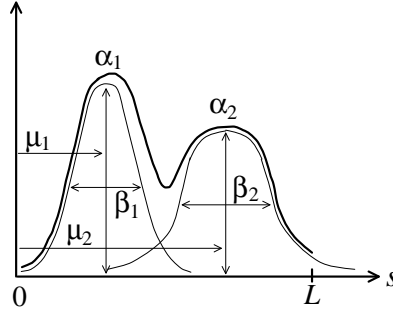


Fig. 14 Examples of Gaussian function and the integrated function

### 3.3 Optimization method

The optimization problem (16) is solved by means of the particle swarm optimization (PSO). The PSO developed by Kennedy and Eberhart in 1995 is one of the population-based stochastic optimization techniques inspired by social behavior of bird flocking. In recent years, PSO has been successfully applied in many research and application areas (Behera and Choukiker 2010, Mauro *et al.* 2009). In the PSO, each candidate for the solution of the problem corresponds to a point in the search space. These candidates are called particles. Each particle also has an associated velocity that decides the next position of its movement. At each iteration, each of the particles changes its velocity and direction taking its best position and the group best position into account. The velocity  $\mathbf{v}$  and position  $\mathbf{x}$  of the particle  $i$  are updated according to Eqs. (17) and (18).

$$\mathbf{v}_i^{(k+1)} = w^{(k)} \mathbf{v}_i^{(k)} + c_1 r_1^{(k)} (\mathbf{p}_i^{(k)} - \mathbf{x}_i^{(k)}) + c_2 r_2^{(k)} (\mathbf{p}_{g,i}^{(k)} - \mathbf{x}_i^{(k)}) \quad (17)$$

$$\mathbf{x}_i^{(k+1)} = \mathbf{x}_i^{(k)} + \mathbf{v}_i^{(k+1)} \quad (18)$$

In the above,  $w^{(k)}$  is the time-varying inertia weight, the coefficients  $c_1$  and  $c_2$  are constants,  $r_1$  and  $r_2$  are two random variables applied independently to provide uniform distributed numbers in the interval  $[0,1]$ ,  $\mathbf{p}_i^{(k)}$  is the position of the best result of particle  $i$ ,  $\mathbf{p}_{g,i}^{(k)}$  is the position of the best global particle in the group, and superscript  $k$  refers to the iteration number. The inertia weight  $w$  decreases by the following manner

$$w^{(k)} = w_{\max} - \frac{w_{\max} - w_{\min}}{k_{\max}} k \quad (19)$$

where  $w_{\max}$  and  $w_{\min}$  are the maximum and the minimum values of inertia weight. The constant  $k_{\max}$  is the maximum number of iteration.

In order to apply the PSO to the multi-objective problem (16), we implement the multi-objective PSO (MOPSO). The important part in the MOPSO is to determine the best global particle  $\mathbf{p}_{g,i}^{(k)}$  for each particle  $i$  of the group. In multi-objective optimization problem each particle of the group should select one of the Pareto-optima as its global best particle. In order to find the best global particle, we use the Sigma method (Mostaghim and Teich 2003). In the paper, the best global

particle is called the best local guide.

In the Sigma method, a vector  $\sigma$  is assigned to each particle in the objective space. Because in the current study the number of objective function is three, we explain the Sigma method in three dimensional space. The value of  $\sigma$  is determined for each particle referring to the coordinate  $(\tilde{J}_1, \tilde{J}_2, \tilde{J}_3)$ . The vector  $\sigma$  is defined as follows

$$\sigma = \frac{1}{\tilde{J}_1^2 + \tilde{J}_2^2 + \tilde{J}_3^2} \begin{bmatrix} \tilde{J}_1^2 - \tilde{J}_2^2 \\ \tilde{J}_2^2 - \tilde{J}_3^2 \\ \tilde{J}_3^2 - \tilde{J}_1^2 \end{bmatrix} \quad (20)$$

Using the basic idea of Sigma method and by considering the objective space, finding the best local guide ( $p_{g,i}^{(k)}$ ) among the Pareto-optima for the particle  $i$  of the group is as follows: In the first step, the vector  $\sigma_j$  is assigned to each particle  $j$  in the Pareto-optimal. In the second step, the vector  $\sigma_i$  for the particle  $i$  of the group is calculated. Then we calculate the distance between the  $\sigma_i$  and  $\sigma_j$ . Finally, the particle  $l$  in the Pareto-optima which  $\sigma_l$  has the minimum distance to  $\sigma_i$  is selected as the best local guide for particle  $i$  during iteration  $k$ . In the case of three dimensional objective space, *closer* means the 3-euclidian distance between the sigma values.

In addition to the Sigma method, we add a turbulence factor (Fieldsend and Singh 2002) to the updated position of each particle in the group. The turbulence factor is implemented as below

$$x_i^{(k+1)} \leftarrow x_i^{(k+1)} + R_T x_i^{(k+1)} \quad (21)$$

where  $R_T$  is a random value in  $[0,1]$  with a constant probability of addition.

In the optimization problem (16), the variables which are independent of each other are randomly generated in the beginning of the optimization process and are modified in each iteration by the Eq. (18). In this problem, the variables to be decided are the coefficients of Gaussian functions in Eqs. (14) and (15). The position  $x$  is represented as the following form.

$$x = \left[ \alpha_{j_h}^h \beta_{j_h}^h \mu_{j_h}^h \alpha_{j_b}^{b_1} \beta_{j_b}^{b_1} \mu_{j_b}^{b_1} \dots \alpha_{j_b}^{b_{N_d}} \beta_{j_b}^{b_{N_d}} \mu_{j_b}^{b_{N_d}} \right] \quad (j_h = 1, \dots, N_h, j_b = 1, \dots, N_b) \quad (22)$$

## 4. Design examples

### 4.1 Setting of parameters for numerical calculation

The parameters used in the optimization are shown in Table 3. The values of the material parameters  $E_1, E_2$  and  $\bar{\sigma}$  are estimated in section 2.3. The applied load vector  $P$  in Fig. 11 is specified as follows:

- magnitude : 121.7 [kN]
- angle from the vertical line : 10° (counterclockwise)
- load applied point : 31-th node

The evaluation item values obtained based on the reference design is shown in Table 4. As explained in section 3.1, the evaluation items  $J_1, J_2$  and  $J_3$  are the structural weight, the sum of the displacement of specified points, and the induced Euclidean norm of the stiffness matrix, respectively.

Table 3 Parameters for numerical calculation

	symbol	value
FE model	Young's modulus: $E_1$	260 [GPa]
	Yield stress: $\bar{\sigma}$	350 [MPa]
	Tangent modulus: $E_2$	8 [GPa]
	Material density: $\rho$	7.87 [g/cm <sup>3</sup> ]
	Number of elements: $N_e$	40
	Number of layers: $N_d$	10
optimization problem	Number of Gaussian function: $N_h, N_b$	10, 4
	Lower bound of size: $h_L, b_L$	5 [mm]
	Upper bound of size: $h_U, b_U$	40 [mm], 50 [mm]
	Upper limit of displacement: $U_{\max}$	40 [mm]
MOPSO	Coefficients: $c_1, c_2$	1.0, 1.0
	Inertia weight: $w_{\max}, w_{\min}$	0.9, 0.4
	Number of particles	3000
	Number of iteration: $k_{\max}$	100
	Probability of adding turbulence factor	0.01

Table 4 Evaluation item values of reference design

$\tilde{J}_1$	$\tilde{J}_2$	$\tilde{J}_3$
1.77 [kg]	7.51 [mm]	$3.80 \times 10^{-7}$ [m/N]

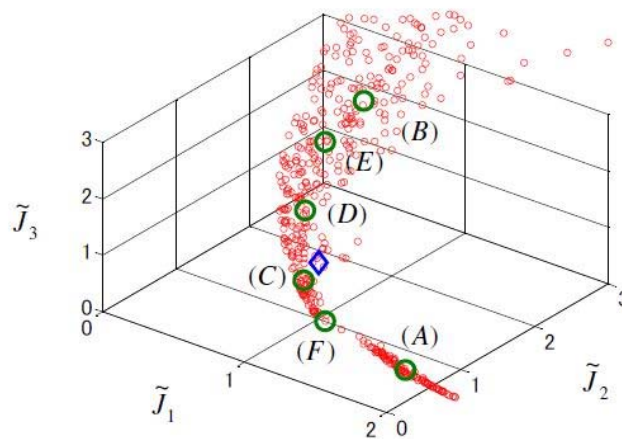


Fig. 15 Result of optimization for the problem (16)

#### 4.2 Obtained results

We present results of optimization and discuss the features of obtained solutions. Fig. 15 shows the result of optimization for the problem (16). A good diversity of solutions is observed. The blue diamond represents the reference design. Each value indicates the ratio to the value of reference design. Fig. 16 shows the distribution of evaluation item values. Figs. 16(a)~(c) plot the

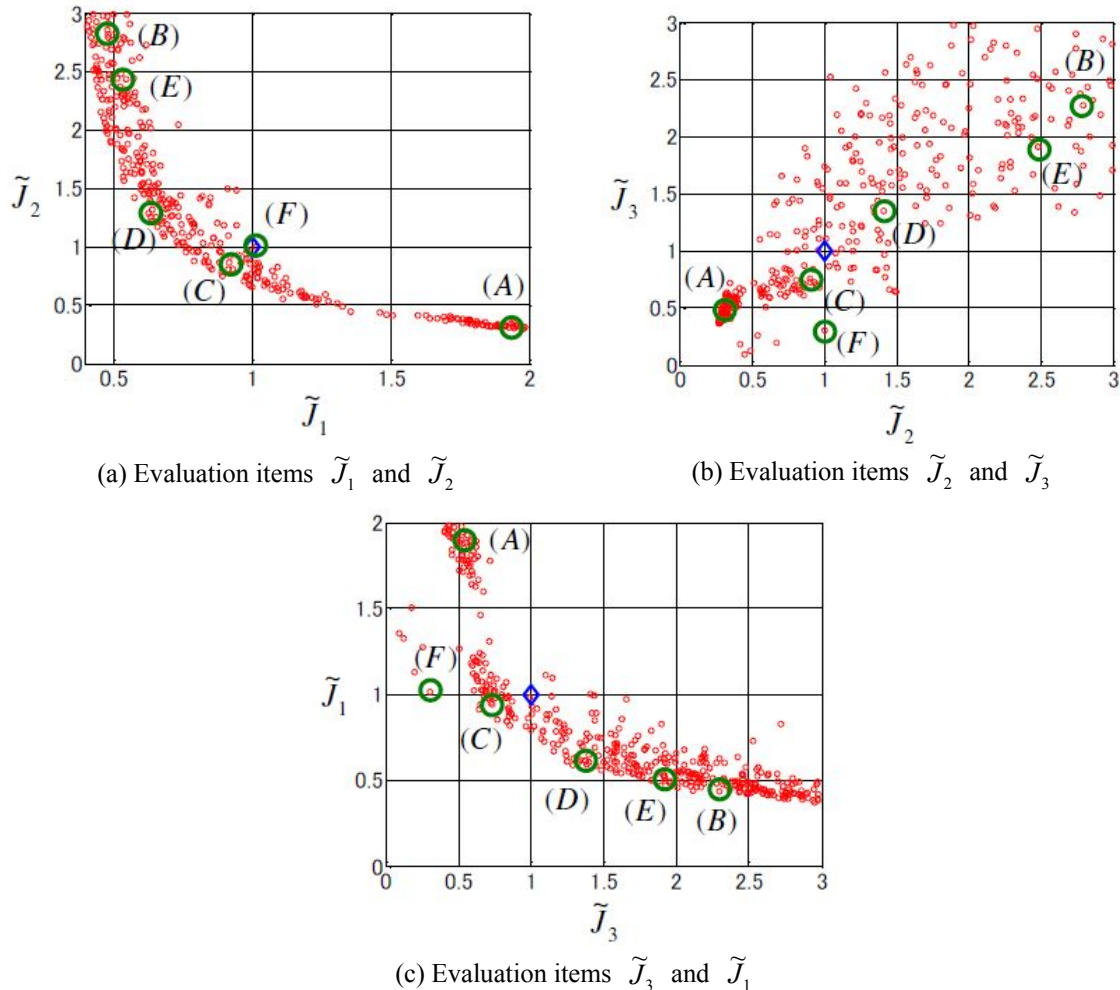


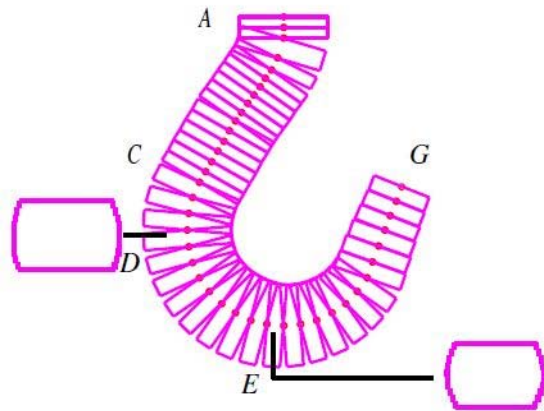
Fig. 16 Distribution of evaluation item values of obtained solutions

pair of  $(\tilde{J}_1, \tilde{J}_2)$ ,  $(\tilde{J}_2, \tilde{J}_3)$  and  $(\tilde{J}_3, \tilde{J}_1)$ . As it is shown in Figs. 16(a) and (c), there are trade-off relationships between the evaluation items  $(\tilde{J}_1, \tilde{J}_2)$  and  $(\tilde{J}_3, \tilde{J}_1)$ . However, the trade-off relationship cannot be observed in Fig. 16(b). There is a positive correlation between the evaluation items  $\tilde{J}_2$  and  $\tilde{J}_3$ . We discuss details about this relation later.

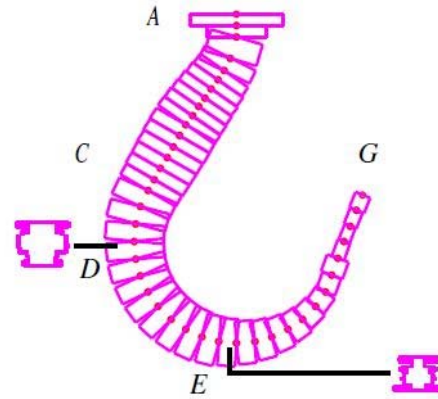
The shapes of the obtained solutions are illustrated in Fig. 17. The central part shows the height distribution of the elements. In the following, we call this part as ‘hook shape’. The selected two cross-sections of design solution are also shown. One is the section of the ‘critical section’ (20th element) and the other is the section of the lower center part (28th element). The top and bottom of the section shape correspond to the inner and outer surfaces of the hook, respectively. These two are important sections in the practical design scene.

The following features are observed for the obtained hook shape:

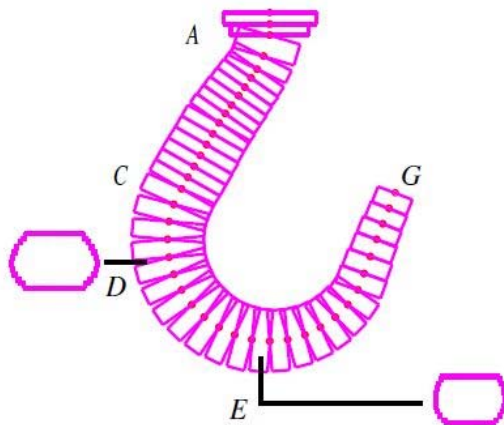
- hook shape becomes thinner toward the tip point “G” from the lower center point “E”
- thickness of base region around the point “A” is greater than any other region (except solution (F))



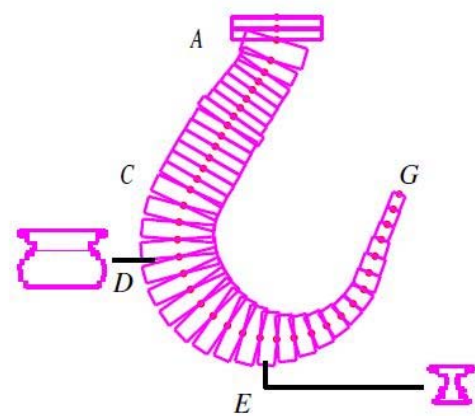
(a) Hook shape and sections of solution (A)  
(good performance on  $\tilde{J}_2$  and  $\tilde{J}_3$ )



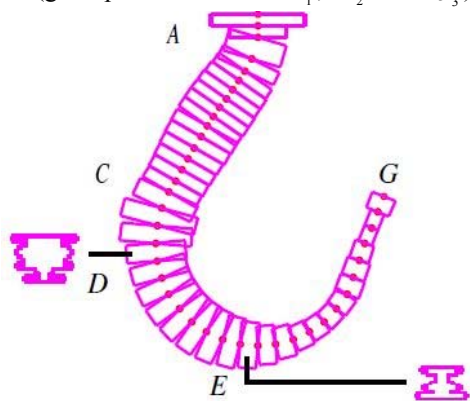
(b) Hook shape and sections of solution (B)  
(good performance on  $\tilde{J}_1$ )



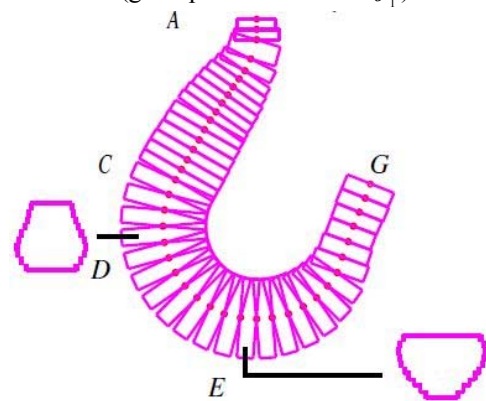
(c) Hook shape and sections of solution (C)  
(good performance on  $\tilde{J}_1$ ,  $\tilde{J}_2$  and  $\tilde{J}_3$ )



(d) Hook shape and sections of solution (D)  
(good performance on  $\tilde{J}_1$ )



(e) Hook shape and sections of solution (E)  
(good performance on  $\tilde{J}_1$ )



(f) Hook shape and sections of solution (F)  
(good performance on  $\tilde{J}_3$ )

Fig. 17 Obtained designs of crane-hook

The larger the attached importance on light weight is, the more remarkable the first feature becomes. Tapering off around the tip point “G” is a rational shape, because the stresses on the surface of hook between the load applied point and the tip point “G” are equal to 0 and this part has no contribution to the strength. On the basis of the mechanical view point, it is better to decrease the thickness of hook from the right part of the load applied point, but the obtained shapes become thinner gradually. The obtained smooth shapes are due to the adopted Gaussian function; they are considered to be practical from the viewpoint of productivity. The obtained shapes have similarity to those of the actual crane-hook design. We can say that the existing designs based on the knowledge empirically obtained by the expert engineers have considerably good performance from the viewpoint of the evaluation items adopted in this study.

We discuss the features of the cross-sectional shape. In the case that we attach importance on light weight, as shown in Figs. 17(b) and (e), the cross-sectional shape is bellows-like shape. The widths between the upper and middle part and the middle and lower part become thinner. This feature is commonly observed at the point “D” and “E”. The width at the point “D” is greater than the width at the point “E”. Since the stress around the point “D” is often larger than that of any other points, larger width is required at this point. If we do not attach importance on light weight, as shown in Figs. 17(a) and (c), the sections of the point “D” and “E” are the rectangular shape whose widths are larger than height. In the case that the importance is attached to the induced Euclidean norm of the stiffness matrix, as shown in Fig. 17(f), the cross-sectional shape of the point “D” becomes thinner toward the top and the shape of the point “E” becomes thinner toward the bottom.

The key points obtained from the observation of the solutions are as follows:

- hook shape is tapering off from the lower center point
- tapering off shape of hook becomes conspicuous as the importance is attached to the light weight
- cross-sectional shape is a wide rectangular in the case that the importance is attached to the strength and the stiffness
- cross-sectional shape is bellows-like in the case that the importance is attached to the light weight

We discuss about the result shown in Fig. 16(b). In this figure, the evaluation items  $\tilde{J}_2$  and  $\tilde{J}_3$  have a positive correlation. In order to confirm the similarity between these two items, we solve single objective optimization problems of  $\tilde{J}_2$  and  $\tilde{J}_3$  with constrained structural weight  $\tilde{J}_1 = 2.0$ . Figs. 18(a) and (b) show the shapes of obtained solutions. The hook shape of Fig. 18(a) has uniform height distribution. The size equals the upper limit. The thicker the hook shape and the cross-sections are, the less the stress of the element becomes. By minimizing the stress, the deformation of hook becomes small. In Fig. 18(b), the thickness of base region around the point “A” is smaller than any other region. The sections are the rectangular shape. In order to keep the high stiffness against not only the downward load but also various loads, this structure is rational. If the applied load condition is unclear, the structure design taking account of the criterion  $\tilde{J}_3$  is important. These two evaluation items have a similar tendency as the objective functions, but the optimal solutions are different from each other. Thus, each of the obtained solutions of the three objective optimization problem has its own significance.

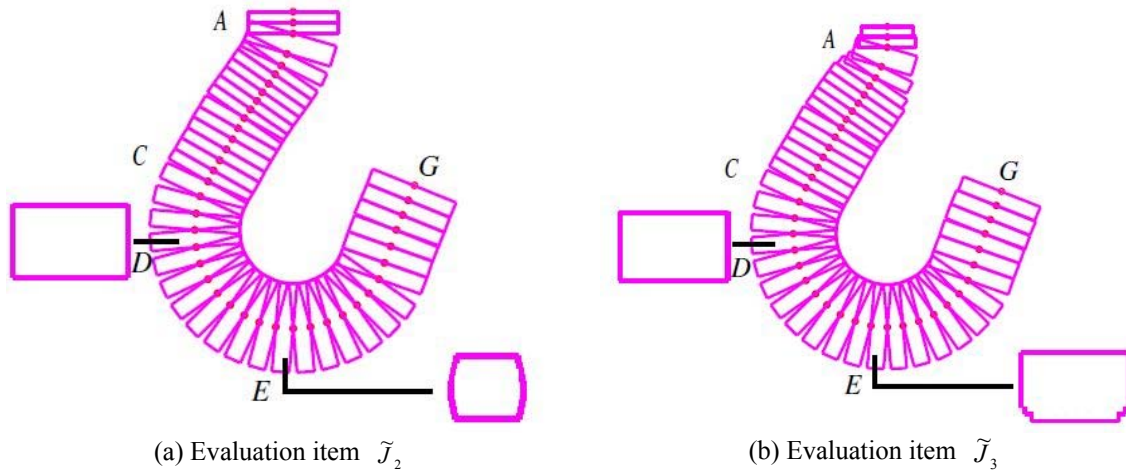


Fig. 18 Obtained designs of crane-hook for single objective problem

## 5. Conclusions

The design and optimization of the crane-hook are presented and discussed. In order to obtain a high-quality design, we formulate the multi-objective optimization problem with three items. The evaluation items are the structural weight, the sum of displacements at the specified points and the robustness against unspecified multiple load conditions. In the representation of the design variables, we utilize the Gaussian functions. The multi-objective problem is solved by means of the MOPSO with the Sigma method.

The obtained crane-hook shapes have a tapered shape similar to those of actual crane-hook designs. This indicates that the evaluation items adopted in this study represent the performance indices of crane-hook that can be adopted in the practical design scenes. Contrary to the similarity in the side view, that is, the height distribution of the elements between the actual design and the obtained designs, the cross-sections are different. The main features of the sections are ‘wide rectangular’ and ‘bellows-like shape’. The former feature is observed when the attached importance on the light weight is less. The latter feature is mainly observed when the attached importance on the light weight is greater. By introducing the Gaussian function to represent the design variables, we can reduce the number of design variables and represent the shape functions effectively. We utilize PSO as the optimization algorithm and are able to produce feasible designs. In this study, we do not consider the production cost. The change of cross-sectional shape needs the modification of the production systems. It is necessary to formulate an optimization problem including the constraints about the production costs in our future work.

## Reference

- Behera, S.K. and Choukiker, Y. (2010), “Design and optimization of dual band microstrip antenna using particle swarm optimization technique”, *J. Infrar. Milli. Terahz. Wave.*, **31**, 1346-1354.
- Boyd, J.P. and Wang, L. (2009), “An analytic approximation to the cardinal functions of Gaussian radial basis functions on an infinite lattice”, *Appl. Math. Comput.*, **215**(6), 2215-2223.

- Chris, P.P. and Sara, G. (2001), "Comparison of fuzzy set and convex model theories in structural design", *Mech. Syst. Sig. Pr.*, **15**(3), 499-511.
- Crisfield, M.A. (1991), *Non-linear Finite Element Analysis of Solids and Structure: Volume 1*, John Wiley & Sons.
- Fieldsend, J.E. and Singh, S. (2002), "A multi-objective algorithm based upon particle swarm optimization, an efficient data structure and turbulence", *The 2002 U.K. Workshop on Computational Intelligence*, 34-44.
- Iman, P., Reza, S. and Mansour, S. (2002), "RBF neural network based PI pitch controller for a class of 5-MW wind turbines using particle swarm optimization algorithm", *ISA Tran.*, **51**(5), 641-648.
- Lam, H.F. and Ng, C.T. (2009), "The selection of pattern features for structural damage detection using an extended Bayesian ANN algorithm", *Eng. Struct.*, **30**(10), 2762-2770.
- Marano, G.C., Greco, R. and Sgobba, S. (2010), "A comparison between different robust optimum design approaches: Application to tuned mass damper", *Probab. Eng. Mech.*, **25**(1), 108-118.
- Ravagnani, M.A.S.S., Silva, A.P., Biscaia, Jr. E.C. and Caballero, J.A. (2009), "Optimal design of shell-and-tube heat exchangers using particle swarm optimization", *Ind. Eng. Chem. Res.*, **48**, 2927-2935.
- Mostaghim, S. and Teich, J. (2003), "Strategies for finding good local guides in Multi-objective Particle Swarm Optimization (MOPSO)", *IEEE 2003 Swarm Intelligence Symposium*, 26-33.
- Muromaki, T., Hanahara, K., Tada, Y. and Nishimura, T. (2012), "Estimation of loading conditions of failed crane-hook: an image-based approach with knowledge and simulation", *Int. J. Reliab. Saf.*, **6**(1/2/3), 130-147.
- Owen, D.R.J. and Hinton, E. (1980), *Finite Elements in Plasticity: Theory and Practice*, Pineridge Press Limited, Chapter 5.
- Roger, A.H. and Charles, R.J. (1985), *Matrix Analysis*, Cambridge University Press.
- Srirat, J., Kitayama, S. and Yamazaki, K. (2012), "Optimization of initial blank shape with a variable blank holder force in deep-drawing via sequential approximate optimization", *J. Adv. Mech. Des., Syst., Manuf.*, **6**(7), 1093-1106.
- Vanderplaats, G.N. (1979), "Efficient algorithm for numerical airfoil optimization", *J. Aircraft*, **16**, 842-847.
- Vissarion, P. and Nikos, D.L. (2009), "Vulnerability-based robust design optimization of imperfect shell structures", *Struct. Saf.*, **31**(6), 475-482.
- Xiang, H.J. and Shi, Z.F. (2011), "Vibration attenuation in periodic composite Timoshenko beams on Pasternak foundation", *Struct. Eng. Mech.*, **40**(3), 373-392.
- Ziping, Q., Yuying, X. and Jialing, Y. (2007), "The static displacement and the stress analysis of structures with bounded uncertainties using the vertex solution theorem", *Comput. Method. Appl. Mech. Eng.*, **196**, 4965-4984.